Progress In Electromagnetics Research M, Vol. 56, 169–177, 2017

Simultaneous Energy and Data Wireless Transfer Attenuation in Biological Channel of Deep Implantable Medical Devices: Characteristic Analysis and Modeling

Xueping Li, Yuan Yang*, Ningmei Yu, and Shijie Qiao

Abstract—The scheme of energy and data wireless transmission with the same carrier based on M-ary Differentially-Encoded Amplitude and Phase Shift Keying (MDAPSK) technology is an effective method to implement energy supply and data communication for implantable medical devices. In this paper, based on a large number of finite-difference time-domain simulation analyses, combined with knowledge of the clinical demand for implantable medical devices, the 13.56–402 MHz band is selected as the biological channel frequency band, and attenuation characteristic analysis and mathematical modeling are carried out. Based on massive amounts of simulation data, the Levenberg-Marquardt and general global optimization methods are adopted to build a homogeneous and heterogeneous biological channel model in the aforementioned frequency band. In order to verify the reliability and versatility of the mathematical model, an adult male rabbit is employed for a living implantation experiment. Using a vector network analyzer, different frequency electromagnetic wave receiving efficiencies in different biological channels are measured. The measured data are highly consistent with the simulation data, which fully verifies the rationality of the proposed biological channel model. This work provides a theoretical basis and model reference for the clinical application of an implantable medical device wireless transmission system.

1. INTRODUCTION

With the development of modern medicine and electronic technology, implantable medical devices have been widely used in modern medicine [1–5]. However, implantable medical devices face common challenges in the areas of energy supply and data transmission. With the development of wireless technologies, wireless energy and data transmission has become a trend in implantable medical devices. However, physical space for embedding is often limited for implantable medical devices clinical application. Therefore, a scheme based on M-ary Differentially-Encoded Amplitude- and Phase-Shift Keying (MDAPSK) technology has been put forward to implement energy and data wireless transmission with the same carrier frequency [6].

In order to achieve wireless transmission between vivo and vitro, the optional frequency bands include the Industrial Scientific Medical (ISM) band (13.553–13.567 MHz, 2.4–2.5 GHz, etc.), Medical Implant Communication Services (MICS) criterion (402–405 MHz), and ultra-wideband (UWB) (3.1–10.6 GHz) [7–11]. The goal of this work is to choose an appropriate transmission carrier frequency for synchronous wireless transmission of energy and data for deep implantable medical devices, and based on this frequency, to then carry out attenuation characteristic analysis and mathematical modeling.

Received 21 February 2017, Accepted 27 April 2017, Scheduled 9 May 2017
* Corresponding author: Yuan Yang (762535409@qq.com).
The authors are with the Department of Electronic Engineering, Xi'an University of Technology, Xi'an, Shaanxi, China.

2. MATERIALS AND METHODS

This study was performed in strict accordance with the recommendations in the Guide for the Care. The protocol was approved by the Committee on the Ethics of Animal Experiments of the Fourth Military Medical University (Permit Number: 15012). All surgery was performed under sodium pentobarbital anesthesia, and every effort was made to minimize suffering.

2.1. Finite-Difference Time-Domain Simulation

In this paper, the finite-difference time-domain (FDTD) method is employed to perform biological channel simulation analysis. The FDTD method is an effective method for solving issues with electromagnetic wave (EMW) transmission and reflection in an electromagnetic medium [12–14]. The conductor model provided by FDTD Solutions software (Lumerical.2013b) was used to establish a biological channel simulation model. The model expression is shown in Eq. (1). The effect of different carrier frequencies on biological channel transmission characteristics are indicated by the biological tissue conductivity σ and relative permittivity ε at different frequencies (biological tissue electrical parameters of 10 Hz–100 GHz have been calculated statistically by the Institute for Applied Physics of the Italian National Research Council [15]):

$$\varepsilon_{total}(f) = \varepsilon + j\frac{\sigma}{2\pi \cdot f\varepsilon_0} \tag{1}$$

The establishment of the simulation model follows the Courant stability criteria, which is expressed as $\Delta t \leq [\delta/(2^{\frac{1}{2}} \times c)]$, where c is the speed of light in vacuum, and $c = 3 \times 10^8$ m/s; Δt is the time resolution of the simulation sampling and δ is the side length of the Yee cell. Taking 6.8 GHz as an example, and setting $\delta = 0.5$ mm, then $\Delta t \leq 1.17$ ps. In this paper, $\Delta t = 0.52$ ps is set.

The homogeneous and heterogeneous biological channel simulation model built by the FDTD simulation software is shown in Figs. 1(a) and 1(b), respectively. During the simulation, EMW source located 3.5 mm from the channel; it is air medium that between EMW source and biological channel, the channel length is 30 mm. For the heterogeneous biological channel simulation model, along the direction of EMW propagation, the channel is composed of 4.5 mm skin, 7.5 mm fat, and 18 mm muscle. In order to prevent electromagnetic wave reflection and refraction effects at the edge of the model, the perfectly matched layer (PML) absorbing boundary is adopted in the modeling process.

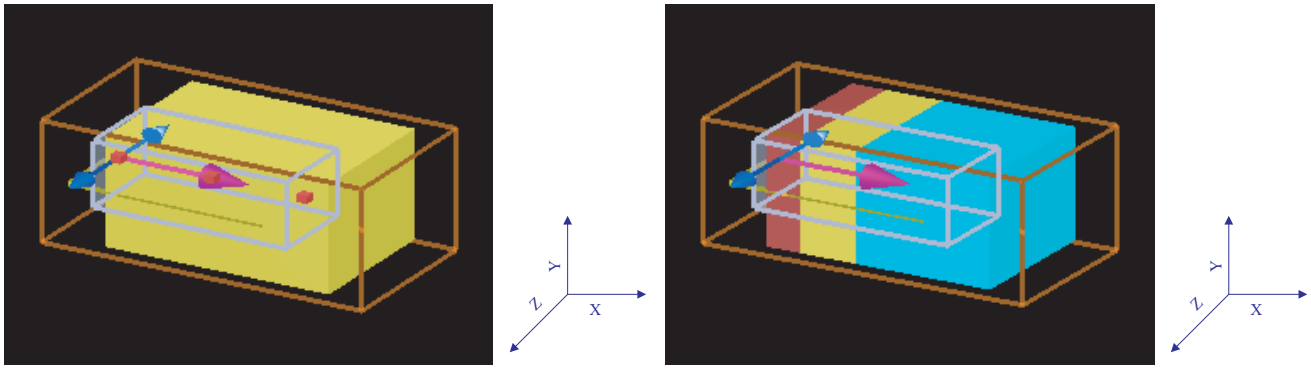

(a) (b)

Figure 1. Biological channel simulation model. (a) Homogeneous biological channel simulation model and (b) heterogeneous biological channel simulation model.

In order to verify the feasibility of the simulation scheme, the 6.8 GHz fat homogeneous channel was taken as an example to analyze the attenuation trend of EMW propagation in homogeneous channels. According to the Beer-Lambert law, EMW strength decreases as propagation depth increases. Thus, the attenuation tendency can be described by [16]:

$$W = W_t \exp(-2\partial d) \tag{2}$$

where W is the EMW energy flux density at any transmission depth of the homogeneous channel, W_t is the EMW incident energy flux density, d is the transmission depth, and ∂ is the channel attenuation coefficient (in unit of [Nep/m]; the latter can be expressed as [16]

$$\partial = \omega \left[\left(\frac{\mu\varepsilon}{2} \right) \left(\sqrt{1 + \frac{\sigma^2}{\varepsilon^2\omega^2}} - 1 \right) \right]^{1/2} \tag{3}$$

The incident energy flux density of the EMW was randomly set as $0.0021\,\mathrm{W/m^2}$. In the 6.8 GHz fat homogeneous channel, according to the Beer-Lambert law, the EMW decay curve is shown as curve 1 in Fig. 2. According to the FDTD simulation model shown in Fig. 1(a), the EMW decay trend is shown as a dotted curve 2 in Fig. 2. From the figure, it can be seen that the two curves coincide well with each other, which verifies the correctness of the modeling approach in this paper.

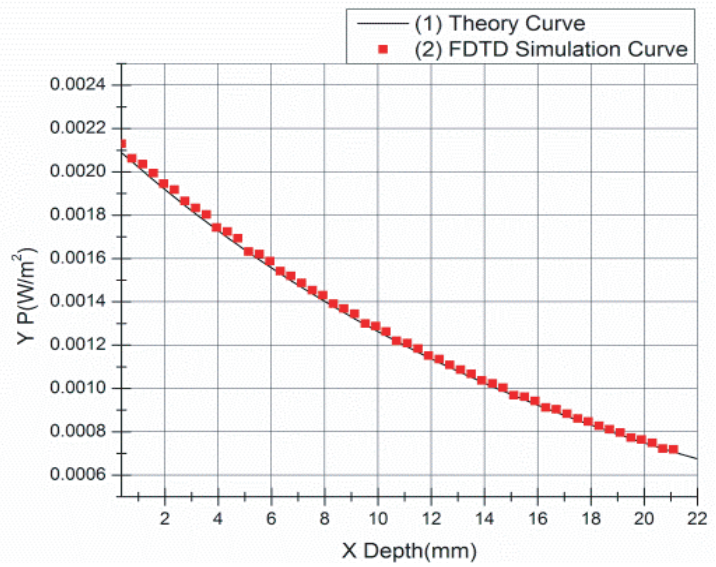

Figure 2. Comparison of FDTD simulation curve and theoretically calculated curve.

2.2. Biological Channel Attenuation Characteristic Analysis at Different Frequencies

Multifrequency-point simulation experiments have been carried out by our research group, and based on those, in this paper, four typical frequencies (13.56 MHz, 402 MHz, 2.457 GHz, and 6.8 GHz) from the Industrial Scientific Medical (ISM) band, Medical Implant Communication Services (MICS) criterion, and ultra-wideband are selected for biological channel EMW attenuation trend analysis. The simulation results at four typical frequencies are shown in Fig. 3, where the x-axis is the depth of the channel in units of mm. The y-axis is the Poynting vector, which indicates the energy flux density of EMW in units of $\mathrm{W/m^2}$. A 21 mm depth of the biological channel is set as the measuring terminal point; the effective heterogeneous channel consists of 4.5 mm skin, 7.5 mm fat, and 9 mm muscle.

From Fig. 3, the following can be seen:

(1) The higher the transmission carrier frequency, the faster the EMW attenuates, which means the signal penetrability in the biological channel is worse;

(2) In the heterogeneous biological channel, at the GHz frequency band as shown in Figs. 3(a) and 3(b), the EMW intensity mutates obviously at the different biological media transition points, while at the MHz frequency band as shown in Figs. 3(c) and 3(d), the mutation is slower than at the GHz frequency band.

The selection of a synchronous energy and data transmission carrier frequency for deep implantable medical devices should balance two aspects of the design requirements for highly efficient energy

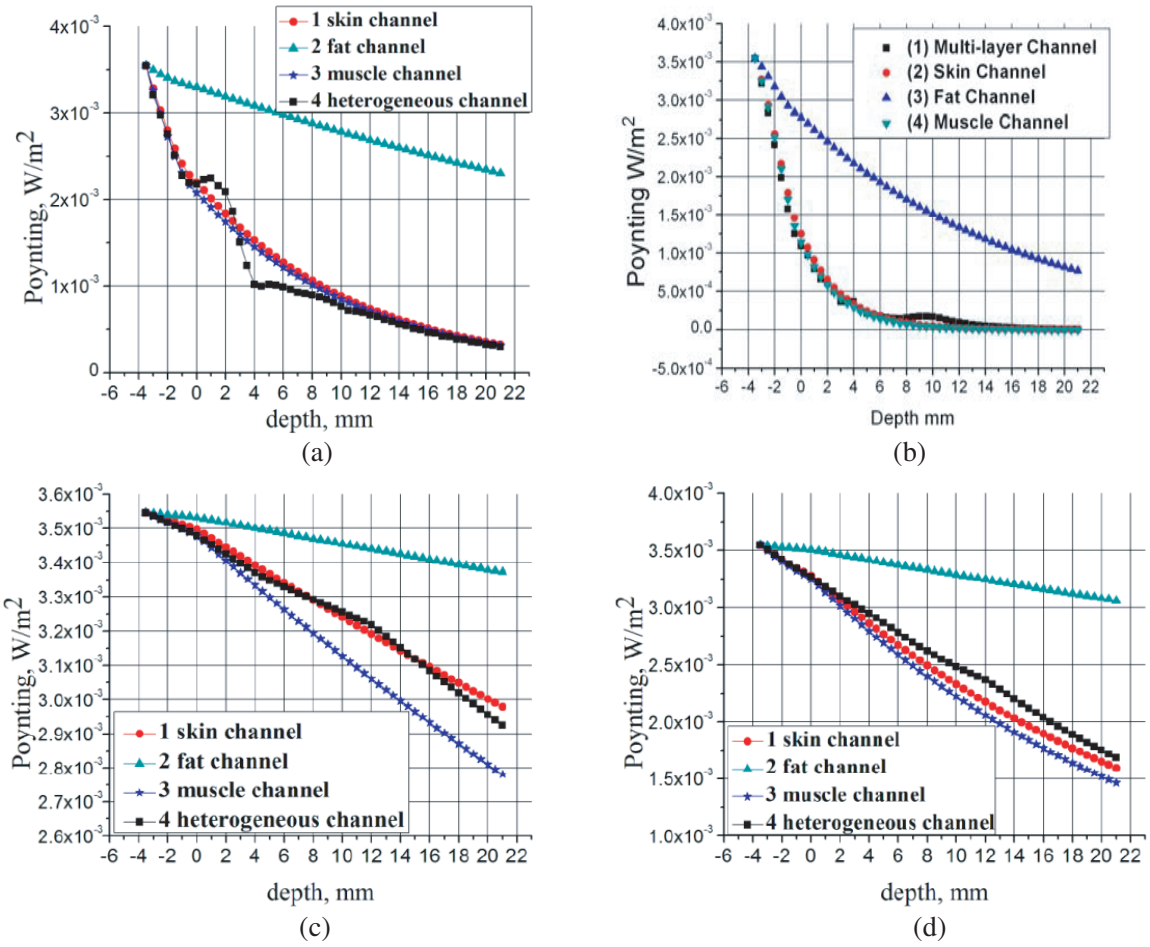

Figure 3. Electromagnetic wave attenuation curves at typical frequencies. (a) 2.457-GHz attenuation curve, (b) 6.8-GHz attenuation curve, (c) 13.56-MHz attenuation curve, and (d) 402-MHz attenuation curve.

transmission and high-speed data transmission. In view of the above observations, although the GHz frequency band can give a sufficiently high data transmission rate, due to its poor penetration in a biological medium (where serious energy loss occurs), the GHz frequency band is not suitable for deep implantable medical devices. For the kHz frequency band, the EWM penetration depth can reach a depth of meters, regardless of penetration depth limitations. However, most implantable medical devices have higher transfer rate requirements. For example, the transfer rate for capsule endoscopy should be greater than 10 Mbps [17], and the transfer rate of a multichannel neural signal recording system should be 100 Mbps or even higher [18]. Therefore, the kHz frequency band is not suitable for a wireless data transmission carrier frequency for implantable medical devices. Thus, the frequency range selected in this paper is limited to the MHz band. Previous literature indicates that when carrier frequency $f = 11.61$ MHz, through circuit optimization the energy transfer efficiency can reach 88.01% [19], which meets the design requirement for high-efficiency energy transmission. At the same time, based on MDAPSK technology, $\log_2^M$ times (where M is modulation order) the data transmission rate of the carrier frequency can be obtained. Therefore, one can simultaneously meet the requirements of energy transmission efficiency and data transmission rate for deep implantable medical devices by selecting a suitable combination of carrier frequency f and modulation order M.

From the simulation results in the MHz band, it is found that, at the low frequency of the MHz band, the EMW attenuation trend in the homogeneous biological channel is linear; in the heterogeneous channel, the attenuation trend is also linear in each type of biological tissue, but the attenuation slope

changes at the different biological media transition points, as shown in Fig. 3(c). As the carrier frequency increases, regardless of whether the biological channel is homogeneous or heterogeneous, the EMW linear attenuation trend deteriorates. As shown in Fig. 3(d), the EMW attenuation trend presents as approximately linear at 402 MHz. In order to consider the accuracy and practicality of the model, the 13.56–402 MHz band was selected for biological channel analysis and mathematical modeling. This band contains multiple ISM and MICS frequencies, which has a wide range of scientific research and medical application value.

3. RESULTS AND DISCUSSION

3.1. Mathematical Modeling of Homogeneous Biological Channel Attenuation Characteristics

After obtaining a very large amount of FDTD simulation data on biological channel attenuation, the Levenberg-Marquardt and general global optimization methods are used to perform surface fitting. Owing to the characterization of different biological tissues by the characteristic electrical parameters of the conductivity σ and relative permittivity ε in biological channel simulation models, σ and ε are selected as independent variables for homogeneous biological channel mathematical modeling. In addition, the intensity of the incident electromagnetic wave, which is indicated by energy flux density P in this paper, has a direct influence on the rate of signal attenuation. The mathematical model of the homogeneous biological channel linear attenuation slope K is obtained as

$$K{=}P * \left(\sum_{i=1}^{n} \left[p_i \sigma^i + q_i \left(\ln \varepsilon \right)^i \right] + m \right), \quad n = 1, 2, \ldots, 5, \tag{4}$$

where p_i, q_i, and m are constant, as shown by the following values:
$p1 = -0.0531$, $p2 = -1.3092$, $p3 = 4.8602$, $p4 = -6.2840$, $p5 = 2.7651$, $q1 = 0.7012$, $q2 = -0.4614$, $q3 = 0.1434$, $q4 = -0.0208$, $q5 = 0.0011$, $m = -0.4076$.

The fitting effect can be measured according to the following parameters: Both the sum of square error (SSE) 2.3262×10^{-6}, and the root of mean square error (RMSE), 1.3752×10^{-4}, tend to be 0. The correlation coefficient (R), 0.9998, and R-squared, 0.9998, both tend to be 1. The above parameters indicate that the fitting method adopted in this paper is reasonable, and, moreover, that the homogeneous biological channel mathematical model established in this paper can accurately reflect the EMW attenuation trend.

3.2. Mathematical Modeling of Heterogeneous Biological Channel Attenuation Characteristics

Within the frequency band studied in this paper, from 13.56 to 402 MHz, there are mutations at the different biological media transition points. However, within each type of biological media, the attenuation slope stays monotonically linear. Therefore, the purpose of heterogeneous biological channel modeling in this paper is to discover an EMW attenuation rule for every type of biological tissue within a specific frequency band.

There are many factors that influence the attenuation slope in each type of biological tissue of a heterogeneous channel, including the electrical characteristic parameter of biological tissue media before and after mutation and the incident electromagnetic energy flow density P. On the basis of the above homogeneous biological channel model, and using a similar mathematical optimization method, the relationship between the normalized EWM attenuation slope of the mutated biological tissue and that of the biological tissue before and after mutation can be obtained. K_f and K_b indicate the homogeneous biological channel attenuation slope before and after mutation, respectively. The slope of biological tissue in the heterogeneous channel is indicated K' to distinguish it from K, the homogeneous biological channel attenuation slope. Through massive simulation data fitting, any biological tissue layer attenuation slope K' in the heterogeneous channel can be calculated by

$$K' = P \cdot \left(\frac{-0.0029 + \mathrm{a}_1 \cdot K_f + a_2 \cdot K_b + a_3 \cdot K_f^2 + a_4 \cdot K_b^2 + a_5 \cdot K_f K_b}{1 + b_1 \cdot K_f + b_2 \cdot K_b + b_3 \cdot K_f^2 + b_4 \cdot K_b^2 + b_5 \cdot K_f K_b} \right) \tag{5}$$

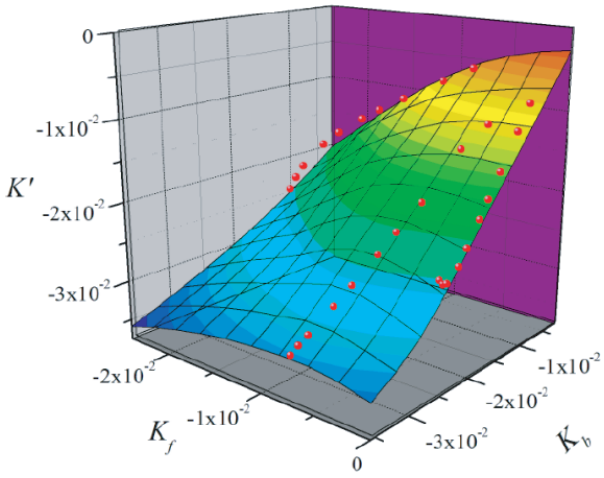

Figure 4. Comparison of 3D curved surface data and FDTD simulation data.

where, a, b are constant, as shown by the following values:
$a1 = -0.0305$, $a2 = 0.6757$, $a3 = -21.6273$, $a4 = 28.8335$, $a5 = -3.3789$, $b1 = -6.4358$, $b2 = 46.1803$, $b3 = -135.8769$, $b4 = 357.883$, $b5 = -64.5874$.

Assuming that $P = 1$, according to the formula (4), the three-dimensional (3D) curved surface data can be plotted as shown in Fig. 4, which also shows FDTD simulation data at 10 random frequency points. It can be seen that the simulation data are highly coincident with the 3D curved surface data with a maximum error of less than 10%. Therefore, the reliability of the heterogeneous biological channel model is fully verified.

3.3. Experimental Validation

In order to verify the reliability of the mathematical models, an adult male New Zealand White Rabbit was employed, on which an implantation procedure was performed on the right side of the groin. 1% pentobarbital sodium was used to narcotize in surgery (dose: 30 mg/kg). A wireless transmission secondary coil was implanted in skin layer, fat layer and muscle layer at different depth, and a primary coil was placed on the surface of the skin. A vector network analyzer (VNA) was used to measure parameter S_{21}, the signal attenuation reflection in the biological channel. After the experiment, the rabbit was euthanasia. At last, the rabbit was package and burned. The following three experiments were performed:

Experiment 1: A secondary coil was implanted into the groin at a depth of 3 mm. The heterogeneous biological channel consists of 1 mm skin and 2 mm fat. When a wireless transmission frequency of 100 MHz was selected, the VNA showed a secondary coil energy receiver efficiency of −9.32 dB (11.69%). According to the early resonance coupling wireless energy transmission model [20], the transmission efficiency without considering the biological channel attenuation should be 16.38% in this situation, so the heterogeneous biological channel attenuation should be 4.69%.

Experiment 2: A secondary coil was implanted into the groin at a depth of 8 mm. The heterogeneous biological channel consists of 1 mm skin, 4 mm fat, and 3 mm muscle. When a wireless transmission frequency of 50 MHz was selected, the VNA showed an energy receiver efficiency of −5.11 dB (30.83%). According to the literature [20], the transmission efficiency without considering the biological channel attenuation should be 42.1%, so the heterogeneous biological channel attenuation should be 11.27%.

Based on the heterogeneous biological channel model proposed in this paper, the EMW biological channel attenuation situation is shown in Table 1 (P_{in} is the normalized strength of the incident EMW). The heterogeneous biological channel attenuation at 100 and 50 MHz is 4.48% and 10.41%, respectively, which basically agrees with the experimental data of 4.69% and 11.27%, respectively.

Experiment 3: The skin and fat layers were peeled, and the muscle tissue was exposed. 13.56 MHz was selected as wireless transmission carrier frequency, and then the wireless energy transmission

Table 1. Electromagnetic wave biological channel attenuation situation.

Frequency (MHz)	Skin layer (mm)		Fat layer (mm)		Muscle layer (mm)		Attenuation (%)
	P_{in}	K'	P_{in}	K'	P_{in}	K'	
100	1		2				4.48
	1	−0.0189	0.9811	−0.013			
50	1		4		3		10.41
	1	−0.0147	0.9853	−0.0093	0.9481	−0.0177	

efficiency in the muscle homogeneous channel was measured at 3, 8, 11, 14, and 18 mm. The comparison of measurement data and simulation data is shown in Fig. 5, in which the x-axis is the channel depth (in units of mm) and the y-axis is transmission efficiency.

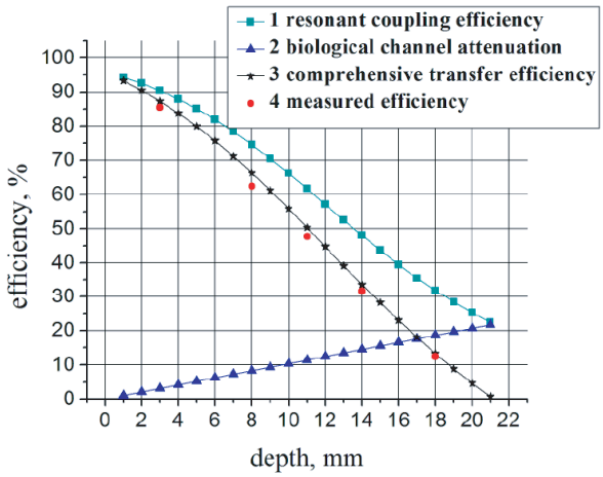

Figure 5. Comparison of measurement and simulation data.

In Fig. 5, curve 4 indicates efficiency measurements at five different depths. Curve 1 indicates calculated efficiency values according to the early resonance coupling wireless energy transmission model without considering the biological channel attenuation [20]. It is found that the error between curve 4 and curve 1 increases with the increase of channel depth. Curve 2 indicates biological channel attenuation according to the mathematical model proposed in this paper. Curve 3 is the difference between curves 1 and 2; thus, resonant coupling transmission loss and biological channel loss are combined in curve 3. Obviously, curves 4 and 3 are highly consistent, fully validating the rationality and reliability of the biological channel mathematical modeling proposed in this paper.

4. CONCLUSIONS

In order to reduce the pain of patients from replacing implantable medical devices cell many times over a lifetime, wireless energy supply and data transmission technology has been widely adopted. The wireless transmission scheme based on MDAPSK realizes wireless energy and data transmission using the same carrier frequency. This scheme can balance implant-unit volume limitations against energy transmission efficiency and data transfer rate. In this paper, through FDTD simulation data analysis employing a large number of frequency points, the suitable carrier frequency band (13.56–402 MHz) for the MDAPSK scheme was selected. In order to further understand the biological channel attenuation features in this frequency band, the Levenberg-Marquardt method and general global optimization methods were used to create homogeneous and heterogeneous biological channel mathematical models. The models were verified by implantation experiments on a living animal. VNA measurement data from the implantation

experiments are highly consistent with the calculation results using the mathematical model proposed in this paper. The frequency band selected and the biological channel attenuation model described herein can provide a theoretical and model reference for the clinical application of implantable medical devices.

ACKNOWLEDGMENT

This work was supported by the National Natural Science Foundation of China (No. 61102017) and Doctorial Innovation Fund of Xi'an University of Technology (No. 310-11202j406), Natural science special project of Shaanxi Province Education Department (No. 16JK1576). We thank LetPub (www.letpub.com) for its linguistic assistance during the preparation of this manuscript.

REFERENCES

1. Demosthenous, P., C. Pitris, and J. Georgiou, "Infrared fluorescence-based cancer screening sapsule for the small intestine," *IEEE Transactions on Biomedical Circuits and Systems*, Vol. 10, 467–475, 2016.
2. Lee, C., H. Choi, G. Go, S. Jeong, S. Y. Ko, J.-O. Park, et al., "Active locomotive intestinal capsule endoscope (ALICE) system: A prospective feasibility study," *IEEE/ASME Transactions on Mechatronics*, Vol. 20, 2067–2074, 2015.
3. Luo, Y. H.-L. and L. da Cruz, "The Argus® II retinal prosthesis system," *Progress in Retinal and Eye Research*, Vol. 50, 89–107, 2015.
4. Bradshaw, P. J., P. Stobie, M. W. Knuiman, T. G. Briffaa, and M. S. Hobbs, "Life expectancy after implantation of a first cardiac permanent pacemaker (1995–2008): A population-based study," *International Journal of Cardiology*, Vol. 190, 42–46, 2015.
5. Sun, T. J., X. Xie, G. L. Li, Y. K. Gu, Y. D. Deng, and Z. H. Wang, "Integrated omnidirectional wireless power receiving circuit for wireless endoscopy," *Electronics Letters*, Vol. 48, 907–908, 2012.
6. Yang, Y., X. Li, and Y. Gao, inventor, Xi'an Hongli patent office, assigned, Implantable visual prosthesis nerve stimulator, China patent CN201210402679.8. 2012 Oct. 22.
7. Bahrami, H., S. Abdollah Mirbozorgi, L. A. Rusch, and B. Gosselin, "Biological channel modelling and implantable UWB antenna design for neural recording systems," *IEEE Transactions on Biological Engineering*, Vol. 62, 88–98, 2015.
8. Li, X., C.-Y. Tsui, and W.-H. Ki, "A 13.56 MHz wireless power transfer system with reconfigurable resonant regulating rectifier and wireless power control for implantable medical devices," *IEEE Journal of Solid-State Circuits*, Vol. 50, 978–989, 2015.
9. Ba, A., M. Vidojkovic, K. Kanda, N. F. Kiyani, M. Lont, X. Huang, et al., "A 0.33 nJ/bit IEEE802.15.6/proprietary MICS/ISM wireless transceiver with scalable data rate for medical implantable applications," *IEEE Journal of Biomedical and Health Informatics*, Vol. 19, 920–929, 2015.
10. Cruz, H., H.-Y. Huang, S.-Y. Lee, and C.-H. Luo, "A 1.3 mW low-IF, current-reuse, and current-bleeding RF front-end for the MICS band with sensitivity of −97 dBm," *IEEE Transactions on Circuits and System*, Vol. 62, 1627–1636, 2015.
11. Alrawashdeh, R. S., Y. Huang, M. Kod, and A. A. B. Sajak, "A broadband flexible implantable loop antenna with complementary split ring resonators," *IEEE Antennas and Wireless Propagation Letters*, Vol. 14, 1506–1509, 2015.
12. Alisoy, H. Z., S. Barlaz Us, and B. B. Alagoz, "An FDTD based numerical analysis of microwave propagation properties in a skin-fat tissue layers," *Optik*, Vol. 124, 5218–5224, 2013.
13. Ha, S.-G., J. Cho, J. Choi, H. Kim, and K.-Y. Jung, "FDTD dispersive modeling of human tissues based on quadratic complex rational function," *IEEE Transactions on Antennas and Propagation*, Vol. 61, 996–999, 2013.
14. Karwowski, A., "Improving accuracy of FDTD simulations in layered biological tissues," *IEEE Microwave and Wireless Components Letters*, Vol. 14, 151–152, 2004.

15. Gabriel, S., R. W. Lau, and C. Gabriel, "The dielectric properties of biological tissues: II. Measurements in the frequency range 10 Hz to 20 GHz," *Physics in Medicine & Biology*, Vol. 41, No. 11, 2251–2269, 1996.
16. Stratton, J. A., *Electromagnetic Theory*, McGraw-Hill Book Company Inc, New York, 1941.
17. Khaleghi, A., R. Chavez-Santiago, and I. Balasingham, "Ultrawideband pulse-based data communications for medical implants," *IET Communications*, Vol. 4, 1889–1897, 2010.
18. Chae, M. S., Z. Yang, M. R. Yuce, L. Hoang, and W. Liu, "A 128-channel 6 mW wireless neural recording IC with spike feature extraction and UWB transmitter," *IEEE Transactions on Neural System and Rehabilitation Engineering*, Vol. 17, 312–321, 2009.
19. Li, X., Y. Yang, Y. Gao, and S. Qiao, "Visual prosthesis wireless power transfer system modeling based on biological capacitance and its efficiency-optimization," *Acta Electronica Sinica*, Vol. 43, 104–110, 2015.
20. Li, X., Y. Yang, and Y. Gao, "Visual prosthesis wireless energy transfer system optimal modelling," *BioMedical Engineering Online*, Vol. 13, 1–11, 2014.